Neurobiology of Disease 132 (2019) 104538

Contents lists available at ScienceDirect

Neurobiology of Disease

journal homepage: www.elsevier.com/locate/ynbdi

Research Paper

Cranial burr hole with erythropoietin administration induces reverse arteriogenesis from the enriched extracranium

Geun Hwa Park[a], Hee Sun Shin[a], Eun Sil Choi[a], Bok Seon Yoon[b], Mun Hee Choi[b], Seong-Joon Lee[b], Kyung-Eon Lee[c], Jin Soo Lee[a,b], Ji Man Hong[a,b,*]

[a] Department of Biomedical Sciences, Ajou University Graduate School of Medicine, Suwon, South Korea
[b] Department of Neurology, Ajou University School of Medicine, Ajou University Medical Center, Suwon, South Korea
[c] Department of Life and Nanopharmaceutical Sciences, Kyung Hee University School of Pharmacy, Seoul, South Korea

ARTICLE INFO

Keywords:
Angiogenesis
Arteriogenesis
Erythropoietin
Ischemic stroke
Cranial burr hole

ABSTRACT

It is challenging to revitalize ischemic penumbra after an acute stroke with intracranial perfusion insufficiency. To evaluate whether cranial burr hole and erythropoietin (EPO) generate effective revascularization, we investigated the efficacy of the augmentation method for reverse arteriogenesis from the healthy extracranial milieu. An intracranial perfusion insufficiency was created through bilateral internal carotid artery ligation (bICAL) in Sprague-Dawley rats. We administered recombinant human EPO (5000 U/kg) or saline intraperitoneally for 3 days after bICAL. Mechanical barrier disruption (MBD) was performed through a cranial burr hole with small dural cracks in the right hemisphere. The ipsilateral hemisphere with MBD grossly showed vascular networks between the extra- and intra-cranial spaces 2 weeks after the MBD procedure. It also showed significantly increased vessels in the intracranial vasculature adjacent to the MBD region ($p = 0.0006$). The levels of pro-angiogenic and inflammatory factors with prominent markers of vessel permeability were also significantly increased (MBD-only vs. control; *Tnf-α*, $p = 0.0007$; *Vegf*, $p = 0.0206$). In the EPO-administered group, such elevations in inflammation were significantly mitigated (combined vs. MBD-only; *Tnf-α*, $p = 0.0008$). The ipsilateral hemisphere with MBD-EPO (vs. MBD-only) showed significantly increased vessels (RECA-1, $p = 0.0182$) and their maturation (RECA-1/α-SMA, $p = 0.0046$), with upregulation of tumor growth factor-β1 (*Tgf-β1*, $p = 0.037$) and matrix metalloproteinase-2 (*Mmp-2*, $p = 0.0488$). These findings were completely blocked by minocycline (MIC) administration during in vivo (*Tgf-β1*, $p = 0.0009$; *Mmp-2*, $p < 0.0001$) and in vitro experiments (tube formation, $p < 0.0001$). Our data suggest that the MBD procedure (for angiogenic routes) and EPO administration (for an arteriogenic booster) are complimentary and can facilitate successfully "reverse arteriogenesis" in subjects with intracranial perfusion insufficiency.

1. Introduction

Abrupt interruption of cerebral blood flow (CBF) by acute stroke can lead to irreversible tissue damage by failure of cerebral autoregulation and impairment of metabolic compensation (Dirnagl et al., 1999). Therapeutic restorative strategies have been reported in stroke victims, including neurogenesis, synaptogenesis, enhancement of neuronal and synaptic plasticity, and augmentation of angiogenesis (Adams Jr. and Nudo, 2013). Among them, angiogenesis has been rarely addressed in the acute period (Liu et al., 2014; Zhang and Chopp, 2009). Rapid reinforcement of arteriogenesis (matured vessel formation) as a reverse mode like bypass surgery, which can supply sufficient oxygen and glucose, is an alternative strategy even in acute stroke for salvaging the ischemic penumbra from the enriched extracranial tissue environment (Pandey and Steinberg, 2011). Anatomically, there is a type of cranial barrier between the extracranial and intracranial environments that mechanically and biochemically protects the vulnerable brain.

Mechanical barrier disruption (MBD) of the protective layers between the intracranial and extracranial arterial systems, which includes the formation of cranial burr holes and small disruptions in the meninges, is a minimally invasive indirect revascularization procedure (Hong et al., 2018). Some clinical studies have reported that cranial

Abbreviations: EPO, erythropoietin; MBD, mechanical barrier disruption; bICAL, bilateral internal carotid artery ligation; TGF-β1, tumor growth factor-β1; MMP-2, matrix metalloproteinase-2; MIC, minocycline

* Corresponding author at: Department of Neurology, School of Medicine, Ajou University, 164, World cup-ro, Yeongtong-gu, Suwon-si, Gyeonggi-do 16499, South Korea.
E-mail address: dacda@hanmail.net (J.M. Hong).

https://doi.org/10.1016/j.nbd.2019.104538
Received 29 March 2019; Received in revised form 7 June 2019; Accepted 19 July 2019
Available online 22 July 2019
0969-9961/

burr holes are beneficial in certain progressive cerebrovascular occlusive disorders, like Moyamoya disease (Hong et al., 2018). Despite its simplicity and minimal complication rate under local anesthesia, use of the cranial burr hole procedure has still been limited in clinical situations as there is no guarantee of revascularization and immediate vascular connections. As a consequence, this simple procedure has rarely been used in experimental and clinical situations. With a potential for safe and warrantable arteriogenesis, it can be a versatile revascularization tool that facilitates reverse angiogenesis from the enriched extracranial environment to replacement the intracranial ischemic penumbra (Cuccione et al., 2016).

Erythropoietin (EPO) has been safely used to treat anemia for a long time because it was originally used as a cytokine for systemic erythropoiesis (Brines and Cerami, 2005). Since the central nervous system expresses EPO and its receptor abundantly, exogenous EPO administration exhibited neuroprotective effects in animal stroke models (Jerndal et al., 2010), which has been explained by a reduction in oxidative stress, apoptosis, and inflammation (Bernaudin et al., 2000; Subiros et al., 2012). Several experiments have shown that EPO induces angiogenesis (Wang et al., 2004), exhibiting an angiogenic potential similar to that of vascular endothelial growth factor (VEGF) (Jaquet et al., 2002). One study reported that EPO enhanced coronary arteriogenesis via vessel maturation by increasing shear stress in a myocardial ischemic model (Imazuru et al., 2009).

Moyamoya disease (MMD) or Moyamoya syndrome (MMS) is a rare cerebrovascular disorder characterized by progressive stenosis of the terminal portion of internal carotid arteries (ICAS) (Scott and Smith, 2009). Unlikely in humans, little has been investigated for appropriate animal models that specify hemodynamic issues in the MMD (Hamauchi et al., 2015).

In the present study, we tested two hypotheses: (1) that the MBD procedure would produce a vascular “detour” for reverse arteriogenesis and (2) that EPO pre-treatment in conjunction with the MBD procedure would reinforce vessel maturation in an intracranial ischemia rat model.

2. Materials and methods

2.1. Human subjects

All procedures performed in studies involving human participants were in accordance with the ethical standards of the institutional committee and with the 1964 Helsinki declaration and its later amendments or comparable ethical standard. We conducted a retrospective analysis of patients with suspected Moyamoya disease (MMD) and Moyamoya syndrome (MMS) who enrolled in prospective MMD registry from May 2010 to March 2016. Patients were enrolled and received initial evaluation including magnetic resonance imaging (MRI), perfusion computed tomography (CT), and transfemoral cerebral angiography (TFCA). Inclusion criteria were followings: (1) age ≥ 16 years; (2) acute neurological presentation; transient ischemic attack (TIA) or cerebral infarction within 2 weeks; (3) angiographic findings compatible with diagnostic criteria for MMD or MMS; (4) significant CBF decrease of at least grade II on baseline perfusion CT (Nemoto et al., 2003), and (5) follow-up TFCA performed at 6 months. According to the Suzuki staging with 6 grades for diagnosis and grading of MMD in terms of vascular morphology using TFCA, the ipsilateral angiographic status was modified into 3-level groups (low-level: Suzuki 1 and 2; intermediate-level: Suzuki 3 and 4; high-level: Suzuki 5 and 6). We serially analyzed the patient's functional status with the National Institutes of Health Stroke Scale (NIHSS) and the modified Rankin Scale (mRS). We determined the ‘unstable course’ as worsening or fluctuating NIHSS during admission, or vice versa for the ‘stable course’. As previously described (Hong et al., 2018), we performed intravenous EPO pretreatment and multiple burr hole. After 6 months, the hemispheric revascularization was evaluated with the extracranial approach by TFCA and quantified with the relative revascularization area (RA) (Cho et al., 2014). CT perfusion scans were acquired from a dual-source CT scanner (Somatom Definition Flash, Siemens Healthcare, Germany) and analyzed with a workstation software (Volume perfusion CT Neuro) at baseline and 6 months. The deconvolution algorithm was used to calculate the values of cerebral blood flow (CBF), cerebral blood volume (CBV), time to peak (TTP), and mean transit time (MTT) as a hemispheric averaging technique.

2.2. In vivo experimental design

The animal procotol used in this investigation were approved by the Institutional Animal Care and Use Committee of Ajou University (IACUC 2016-0043). All of experimental procedures were conducted in compliance with the institutional guidelines of the committee. Adult male Sprague-Dawley rats (8 weeks, 260 to 280 g; Orient Bio, South Korea) were used. The rats were anesthetized in an induction chamber with 4% isoflurane, and anesthesia was maintained with 2% isoflurane (IFRAN LIQ, Hana Pharm. Co., South Korea) in a mixture of 30% O_2 and 70% N_2. The rats' body temperature was maintained at 37 ± 0.5 °C throughout the surgery and during recovery by regularly monitoring and adjusting the temperature using a rectal probe with a temperature controller (CMA Microdialysis, USA).

Mild ischemia was induced through permanent bilateral internal carotid artery (ICA) ligation which did not elicit any functional deficits (Ohta et al., 1997). Briefly, after making an incision in the midline of the neck, the bilateral common carotid arteries (CCA) and external carotid arteries (ECA) were carefully exposed and isolated. Then the bilateral ICAs were doubly ligated using 4–0 silk sutures. The rats were randomly assigned into 3 groups (Supplementary Fig. 1 and 2) 1): Control, MBD-only, and Combined ($n = 6$ to 8 for each group). In a blinded manner, animals were administered either recombinant human erythropoietin (EPO) (5000 U/Kg Epokine; CJ HealthCare, South Korea) or saline intraperitoneally for 3 days before the MBD procedure. The following animals were excluded: (1) those with an insufficient reduction of CBF (> 80% of baseline) after bICAL (Supplementary Fig. 3), (2) those with adverse outcomes during the MBD procedure, such as focal bleeding and sudden death during anesthesia (Supplementary Fig. 2). The rats were killed at 1 day, 4 days, 2 weeks, 1 month, and 3 months after the MBD procedure. To investigate the influence of combination therapy on inflammation and MMPs, we used minocycline (MIC) as an inhibitor of both inflammation and MMPs (Garrido-Mesa et al., 2013). The rats were then further randomly assigned into 5 groups (Fig. 6A and Supplementary Fig. 2): Control, MBD-only, MBD-only + MIC, combined, and combined + MIC. Minocycline (45 mg/kg, pH 7.4, Sigma) was injected intraperitoneally into the rats daily until 2 weeks after the MBD procedure. Early gene expression and late angiogenesis were subsequently analyzed.

2.3. Mechanical barrier disruption (MBD)

The anesthetized rat was mounted onto a stereotaxic frame. The MBD procedure was performed by making a cranial burr hole (2.5 mm inner diameter and with center 4 mm right lateral to the bregma) and a small disruption in the dura mater in the right hemisphere. In detail, using a dental drill with foot controller (Saeshin Co., South Korea) at a low speed, we carefully thinned the skull over the landmark defined as the MBD region using stereotaxic coordinates. Moistening the skull with sterile saline facilitated thinning of the skull surface. When the last section of compact bone remained, the pial vessels could be seen through the bone. We carefully drilled through the middle of the hole at a slow speed using the dental drill and then used a rongeur (Fine Science Tool Co., USA) to remove pieces of peripheral bone to fit through the 2-mm inner diameter. Bleeding in the skull or surrounding tissue was stopped by careful cauterization (Bovie Medical Co., Clearwater, FL, USA). After removal of skull completely, we cautiously

made a small incision in the dura mater under the burr hole using a 32-gauge needle syringe. We then placed a rounded micro-point probe at an angle of 90° and removed the dura mater cleanly. Finally, the scalp was carefully closed (see Supplementary Fig. 1A).

2.4. In vivo brain imaging

2.4.1. Measurement of cerebral blood flow (CBF)

Cerebral blood flow (CBF) was measured using a laser Doppler blood perfusion imager (PeriScan PIM3 System; PERIMED, Sweden). Briefly, after incising the scalp of the anesthetized rat on the stereotaxic frame, perfusion recordings of the bilateral cortices were acquired from a $2 \times 2\,cm^2$ field of view at a working distance of 15 cm. The CBF was measured before and after ligation. Colour-coded images of the relative perfusion levels were displayed on a video monitor and all images were analyzed with PIMsoft, a PeriScan PIM3-dedicated software (Primed, Sweden).

2.4.2. Time-of-flight (TOF) magnetic resonance angiography (MRA)

Imaging was performed on a Bruker 9.4 T small animal MR system (ID = 12 cm, Gradient strength = 660 mT/m @ 4570 T/m/s) (Biospec 94/30, Bruker Biospin, Ettlingen, Germany). The radiofrequency (RF) transmission energy (inner diameter = 86 mm) and receive gain were automatically adjusted. The anesthetized rats were placed in the prone position onto an animal holder. Survey scans using gradient-echo fast imaging were performed to gain the accordant symmetrical position. TOF-MRA images were acquired using a three-dimensional (3D) FLASH sequence (TE/TR/FA = 1.608 ms/12 ms/20°, matrix size = 256 × 256 × 280, voxel size = $137 \times 137 \times 100\,\mu m^3$, field of view = $35 \times 35 \times 28\,mm^3$). To suppress the venous signals, a 20-mm-thick saturation band was positioned at the rostral side of the measured slice. MR angiograms were obtained by generating the maximum intensity projection (MIP) using RadiAnt DICOM Viewer software (Medixant, Poznan, Poland).

2.5. Measurement of hematocrit (HCT)

To analyze the impact of EPO administration on the hematocrit (HCT), a 200-μL blood sample was collected sequentially from the tail vein of rats in each group during the study using heparinized capillary tubes.

2.6. Blood-brain barrier (BBB) leakage analysis

To observe the BBB breakdown, we performed BBB leakage analyses at baseline and 1, 4, 7, 9, and 14 days after the procedure. One day before decapitation, the anesthetized rats were injected intravenously with 4% Evans blue (EB) into the tail vein, which was allowed to circulate for 20 to 24 h. The anesthetized rats were perfused transcardially with phosphate buffered saline (PBS) to remove the dye from the blood vessels. The extracted brain was imaged using a stereomicroscope (SMZ745T, Nikon, Japan) equipped with a digital camera. BBB leakage quantification was described by the total area of Evans blue extravasation.

2.7. Microangiography using black India ink and blue dye injections

To visually observe the trans-dural anastomosis, we performed microangiography by administering India ink and blue dye with Evans blue. For systemic circulate, the anesthetized rats were perfused with PBS and 4% PFA, injected transcardially with 3% black ink in gelatin solution without air bubbles, and solidified on ice overnight. Next, by carefully separating the cranial bones, the black trans-dural anastomoses in the MBD region could be observed diagonally using a stereomicroscope (SMZ745T, Nikon, Japan) equipped with a digital camera. For circulation via the ECA, we inserted polyethylene tubes (PE10, Becton-Dickinson, Franklin Lakes, NJ, USA) into the bilateral ECAs of the anesthetized rats in advance. After perfusing with PBS, we injected 100 μL of 3% Evans blue into the polyethylene tube connected to the ECA. Rapid blue coloration of the right side of the mouth, right eye, and right ear confirmed proper placement of the tubes. Within three seconds of observing the blue colour, we decapitated the rats and post-fixed the extracted brains. Images were acquired using a stereo microscope (SMZ745T, Nikon, Japan) equipped with a digital camera.

2.8. Tissue processing and immunohistochemistry

The rats were anesthetized using intraperitoneal injections of a mixture of 75 mg/kg ketamine (Yuhan Co., South Korea) and 10 mg/kg xylazine (Bayer Korea, South Korea). This was transcardially perfused with phosphate buffered saline (PBS), which was fixed in 4% paraformaldehyde (PFA). The brain extracted from skull was post-fixed in 4% PFA and cryoprotected in a series of graded sucrose solutions until the isolated brains sank to the bottom of their containers. Brain tissues frozen in liquid nitrogen were cut coronally into 30-μm-thick sections using a cryostat (CM3050S, Leica, Germany).

For the immunohistochemical analysis, tissue sections mounted on slides were permeabilized in 0.25% triton X-100 in PBS. After washing with PBS, the sections were incubated with 10% normal serum for 1 h and then with primary antibodies overnight at 4 °C under humidified conditions. We used the following primary antibodies: mouse anti-rat endothelial cell antigen-1 (RECA-1, 1:200; Serotec), rabbit anti-α-smooth muscle actin (α-SMA, 1:400; Abcam), and rabbit anti-ionized calcium binding adaptor molecule 1 (Iba1, 1:400; Wako). After washing with PBS, the specimens were incubated with secondary antibodies conjugated with Alexa Fluor 488 or 555 (Invitrogen, Carlsbad, CA, USA) for 2 h at room temperature. Slides were mounted using Vectashield mounting medium (Vector Laboratories, Burlingame, CA, USA). Images were captured using a microscope with Axio Vision 4.7 software and Axio scan Z1 with ZEN software (Zeiss, Jena, Germany). To analyze the antibody-specific signals, NIH Image J software program was used to evaluate the images.

To analyze angiogenesis and vessel maturity at 1 and 3 months after the MBD procedure, we obtained a 200× magnification image of the total cortex including the MBD region, with the center at the site 4 mm lateral to the bregma. Each image was divided into six sections at 400 μm intervals according to its depth from the cortex. Three regions in each section were used for the quantitative analyses. For angiogenesis, the vessel area was assessed as the percentage of the area occupied by RECA-1 positive vessels divided by the total area. For vessel maturity, we first counted the number of RECA-1-positive vessels and the number of RECA-1/α-SMA double-positive vessels per unit area. We next calculated the mature vessels as a percentage of the double positive vessels to the whole vessels. Finally, the results of vessel maturation were expressed by dividing the values for the ipsilateral hemisphere by those of the contralateral hemisphere to obtain the effect of MBD on vessel maturation in the ipsilateral to contralateral regions. To analyze microglia/macrophage activation, we randomly chose four fields of ×200 magnification in the ipsilateral MBD and the contralateral non-MBD regions in all study periods. We quantified the number of Iba-1 positive cells per mm^2 and presented the relative value as the percentage of the ipsilateral cortex to the contralateral cortex.

2.9. RNA extraction and quantitative real time polymerase chain reaction (qRT-PCR)

Sampling were performed at various timeframes (1 day, 4 days, 2 weeks, 1 month, and 3 months) after MBD. cDNA was extracted from the cortical tissue with an MBD region using the Easy-Blue™ Total RNA Extraction kit (iNtRon Biotechnology, South Korea) and the SuperScript® III First-strand Synthesis System (Invitrogen, Carlsbad, CA, USA). Real-time PCR amplifications were performed using

Table 1
Patient (n = 37) and hemispheric (n = 50) profiles associated with sufficient revascularization at 6 month after the procedure.

	Sufficient revascularization[a] (RA ≥ 33%)	Insufficient revascularization (RA < 33%)	P
Patient profiles (n = 37)	(n = 23)	(n = 14)	
Age, n (%)	46.5 ± 12.7	51.9 ± 15.8	0.307
Female, n (%)	15 (65.2)	5 (35.7)	0.081
Associated clinical factors			
Hypertension, n (%)	11 (47.8)	9 (64.3)	0.330
Diabetes mellitus, n (%)	2 (8.7)	5 (35.7)	0.042
Moyamoya disease,[b] n (%)	12 (52.2)	4 (28.6)	0.160
MMD Family history, n (%)	1 (4.3)	2 (14.3)	0.303
Any DWI lesion, n (%)	19 (82.6)	7 (50.0)	0.035
Function outcome			
NIHSS (initial)	2.7 ± 2.9	4.4 ± 6.6	0.400
NIHSS (at discharge)	2.5 ± 3.4	2.5 ± 4.6	0.987
mRS (initial)	1.7 ± 1.3	2.1 ± 1.4	0.367
mRS (6-mo)	1.1 ± 1.0	1.3 ± 1.4	0.615
Hemispheric profiles (n = 50)	(n = 26)	(n = 24)	
Ipsilateral DWI lesion, n (%)	17 (65.4)	11 (45.8)	0.164
Unilateral Moyamoya, n (%)	8 (30.8)	2 (8.3)	0.048
Ipsilateral Basal Moyamoya, n (%)	16 (61.5)	9 (37.5)	0.089
Perfusion parameters			
CBF, ml/100 g/min	39.9 ± 12.9	45.9 ± 12.5	0.131
CBV, ml/100 g	3.02 ± 0.68	2.85 ± 0.61	0.401
TTP, sec	13.6 ± 2.2	11.7 ± 1.8	0.017
MTT, sec	6.4 ± 1.9	4.9 ± 1.2	0.003

RA, revascularization area; DWI, diffusion weighted image; MMD, moyamoya disease; NIHSS, National Institute of Health Stroke Scale; mRS, modified Rankin Scale; CBF, cerebral blood flow; CBV, cerebral blood volume; TTP, time to peak; MTT, mean transit time.

[a] If burrhole procedure is performed bilaterally, the patient was classified as sufficient revascularization if there was sufficient revascularization in any hemisphere.

[b] Moyamoya disease is fully satisfactory with (1) bilateral involvement, (2) steno-occlusive changes at the terminal portion of the ICA, and (3) presence of basal Moyamoya vessel network.

QuantiTect® SYBR® Green PCR Master Mix (Qiagen, Germany) with the indicated primer pairs (Supplementary Table 1). Quantitative RT-PCR was performed on a CFX96 Real-Time PCR Detection System (Bio-rad, Hercules, CA, USA) using three-stage program parameters provided by the manufacturer, as follows: 2 min at 50 °C, 15 min at 95 °C, and then 40 cycles of 15 s at 94 °C, 30 s at 50 to 60 °C, and 30 s at 72 °C. Target mRNA was normalized to the expression level of 18S rRNA generated from the same sample and thereafter related to controls. Relative gene expression was determined using the $2^{-\Delta\Delta CT}$ method.

2.10. In vitro experimental design

In vitro experiments were performed by personnel who were blinded to the in vivo results. Human umbilical vein endothelial cells (HUVECs) (Lonza, Basel, Switzerland) were cultured in endothelial growth medium (EGM-2) (Lonza, Basel, Switzerland) supplemented with 2% fetal bovine serum (FBS). Human aortic smooth muscle cells (HAoSMCs) (Lonza, Basel, Switzerland) were cultured in smooth muscle cell growth medium (SmGM-2) (Lonza, Basel, Switzerland) supplemented with 2% FBS. HUVECs and HAoSMCs between passages 3 and 5 were used for experiments. For expansion, cells were maintained in standard humidified incubators at 37 °C with 5% CO_2, and the culture medium was changed twice a week until 90% confluence was reached.

We found that the optimum dose of EPO associated with maximum angiogenesis in a tube formation assay was 10 IU/mL. Confluent HUVECs were cultured for 24 h under different conditions: control, EPO, EPO and 10 μM minocycline (MIC) (Jung et al., 2014), EPO and 5 μM ARP-100 (MMP-2 specific inhibitor; Cayman Chemical, Ann Arbor, MI, USA) (Jana et al., 2016), and EPO and 10 μM SB431542 (TGF-β1 inhibitor; Cayman Chemical, Ann Arbor, MI, USA) (Ma et al., 2007). In addition, the conditioned media of HUVECs (HUVECs-CM) from each group were selectively collected for assessment of the paracrine factors secreted by the EPO-treated HUVECs (Janmaat et al., 2010). The collected media were then centrifuged at 1500*g* for 10 min and finally filtered using a 0.45-μm syringe filter (Millipore, Bedford, MA, USA).

2.11. Tube formation of HUVECs

A 24-well plate was coated with Matrigel (250 μL, Corning, Bedford, MA, USA) and incubated for 30 min at 37 °C for gel formation. HUVECs from each group were detached with trypsin-EDTA and re-suspended in medium at a concentration of 50,000 cells/well. Cell suspensions were placed on the Matrigel (150 μL/well) and incubated in standard incubators at 37 °C for 24 h to allow for tube formation. After 24 h, the non-integrated cells were washed out and the tube formation on matrigel was photographed using a phase contrast inverted microscope (CKX41, Olympus, Tokyo, Japan) at ×4 magnification. For quantitation, total tube length, the number of branching points, and the number of tube formations were quantified using the Angiogenesis Image Analyzer for Image J software (National Institutes of Health, Bethesda, MD, USA).

2.12. Wound healing of HAoSMCs

HAoSMCs were grown to confluency in SmGM-2 and then replaced with the conditioned medium from EPO-treated HUVECs in the presence or absence of inhibitors. For the wound healing assay, a straight scratch was made in the monolayer using a 200 μL pipette tip and photographed at 0, 4, and 8 h using a phase contrast inverted microscope (CKX41, Olympus, Tokyo, Japan). The extent of wound healing was determined by outlining the wound and measuring the area at different times. Cell migration was also quantified by counting the number of cells that migrated into the scratched area.

2.13. Statistical analysis

All statistical analyses were performed using statistical software IBM SPSS Statistics 22 (Chicago, IL, USA) and Prism version 7.0 (GraphPad Software, La Jolla, CA, USA). Data are expressed as

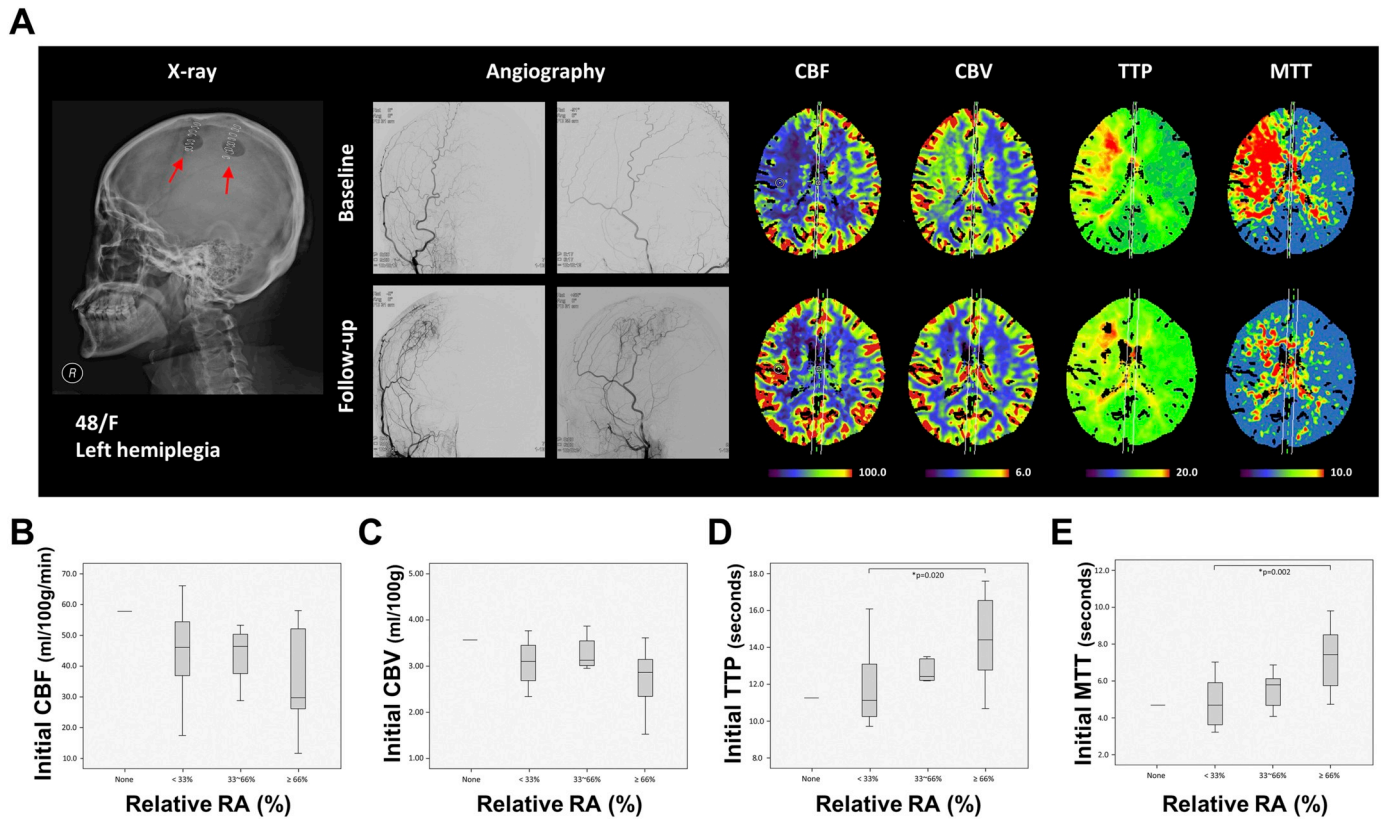

Fig. 1. Reverse arteriogenesis in humans with combination therapy. (A) Representation pictures about the combination therapy in 48-year old woman with left hemiplegia. Angiography and CT perfusion maps (CBF, CBV, TTP, and MTT) at baseline and 6 months after combination therapy. Red arrows indicate MBD region. As compared to baseline status, there were successful transdural revascularization and CBF restoration on 6-month follow up. (B–E) The mean value of initial CBF (B), CBV (C), TTP (D), and MTT (E) according to the 6-month relative revascularization area (RA, %) from 50 hemisphere in 37 patients with the combination therapy. Our study shows that relative RA is significantly associated with time delays (TTP, p = 0.020; MTT, p = 0.002) rather than CBF and CBV values on initial perfusion status. CBF, cerebral blood flow; CBV, cerebral blood volume; TTP, time to peak; MTT, mean transit time; MBD, mechanical barrier disruption; RA, revascularization area.

mean ± standard deviation (SD). To analyze the data statistically, we performed Student's unpaired *t*-test for comparisons between the two groups and a one-way or two-way analysis of variance (ANOVA) for multiple comparisons of each treatment group, with the independent variables being treatment groups and days of testing. These were followed by Tukey's post hoc tests. Statistical significance was set at $p < 0.05$.

3. Results

3.1. Reverse arteriogenesis in humans with combination therapy

We performed the combination therapy over 6 years and included a total of 50 hemispheres from 37 patients in 113 suspected MMD or MMS (Table 1). We followed them for 6 months to observe the newly-formed reverse arteriogenesis (Fig. 1). Compared to the baseline, a successful reverse arteriogenesis and improvement of CT perfusion parameters were observed at 6 months (Fig. 1A). To analyze the relationship between initial evaluation and 6-month revascularizaion, we compared initial CT perfusion parameters (CBF, CBV, TTP, and MTT) according to the angiographic grading of relative revascularizaion area (RA). We observed significant improvements of revascularizaion area in the patients who had initially elongated TTP ($p = 0.020$) and MTT ($p = 0.002$) (Fig. 1D–E). However, there was no difference of the initial CBF and CBV (Fig. 1B–C). These hemodynamic findings suggest that the delayed perfusion is critical prerequisites in determining the success of reverse arteriogenesis by combination therapy.

The mRS of the enrolled patients had a significant improvement after six months (1.8 ± 1.4 at baseline vs. 1.2 ± 1.1 at 6 months; $p < 0.001$ by paired *t*-test). In detail (Supplementary Fig. 4), sequential NIHSS scores during admission were shown according to (A) angiographic status (low-level, intermediated-level, high-level) and (B) clinical course (unstable, stable). As compared to low-level group, the NIHSS values were significantly higher in intermediate-level ($p < 0.001$) and high-level ($p < 0.001$) groups. As compared with low-level group, intermediate-level and high-level groups had a more tendency of unstable clinical course (0.0% vs. 22.2% vs. 16.7%). This point suggests that the efficacy of combination therapy is closely related to target patients with unstable hemodynamics. In terms of the patient's clinical course, neurological fluctuation appeared to occur between 3 and 14 days after hospitalization (3 days, $p = 0.002$; 7 days, $p < 0.001$; 14 days, $p = 0.018$). Therefore, we believe that the combination therapy is a well-timed and minimally-invasive revascularization modality for acute symptomatic patients with perfusion impairment.

3.2. Reverse arteriogenesis using the MBD procedure

We evaluated the possibility of transcranial anastomosis from the extracranial vascular system using the MBD procedure in a mildly ischemic rat model (Fig. 2). To evaluate BBB permeability after MBD, we observed the Evans blue extravasations. Compared to the baseline, extravasation into the ipsilateral hemisphere was markedly increased at 1 day ($p = 0.0093$) and peaked at 4 days ($p < 0.0001$), but it was significantly diminished 2 weeks after MBD (Fig. 2A and Supplementary Fig. 5). To visualize the restoration of the periosteum which was removed during the procedure, the rats were perfused with India ink.

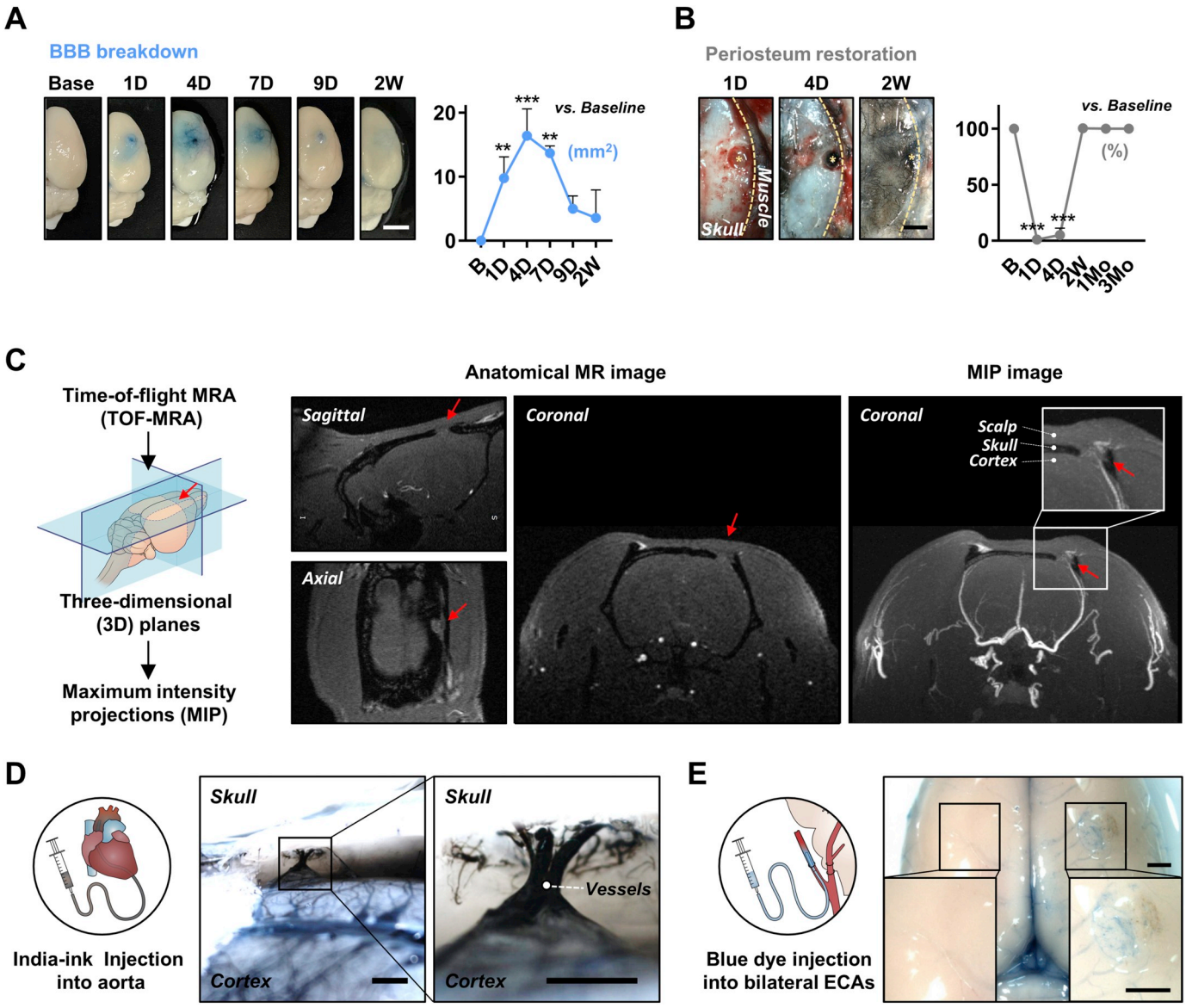

Fig. 2. MBD procedure successfully induces the reverse arteriogenesis from the enriched extracranium. (A) Evans blue (EB) extravasation in ipsilateral MBD hemisphere at baseline, 1 day, 4 days, 7 days, 9 days, and 2 weeks after the MBD procedure (Scale bar, 5 mm; n = 3 to 5 animals per group). (B) Periosteum restoration in ipsilateral MBD hemisphere at 1 day, 4 days, and 2 weeks after the procedure (scale bar, 2 mm; n = 3 animals per group). (C) Anatomical magnetic resonance (MR) and maximum-intensity projection (MIP) images of the rat brain with MBD procedure (red arrows) at 3 months. (D) Postmortem cerebral angiography with transcardial black-gelatin solution injection at 3 months after the procedure. Transdural anastomosis is grossly shown by lifting the rat's skull (Scale bar, 1 mm). (E) Postmortem angiograpy where to be the origin of reverse arteriogenesis in our experimental model, injecting blue dye into bilateral external carotid arteries (ECAs). The residues of blue dye are grossly shown in ipsilateral MBD hemisphere (scale bar, 1 mm). $^{*}p < 0.05$, $^{**}p < 0.01$, $^{***}p < 0.001$. B = baseline; D = day; W = week; Mo = month.

Highly vascular periosteum filled with India ink was restored at 2 weeks, although it was not seen before that (1 day and 4 days: $p < 0.0001$ vs. *baseline*, (Fig. 2B and Supplementary Fig. 6).

To verify the transcranial vascular connections to viable intracranial tissue, we performed TOF-MRA. MRIs showed other tissue connections between the extracranial and intracranial cavities in their respective 3D planes. There was a vascular network on the maximum-intensity-projection (MIP) images of TOF-MRA data as a functional reverse arteriogenesis in the ipsilateral hemisphere (Fig. 2C). Transcranial vessels were observed between the cerebral cortex and the skull at 2 weeks after the MBD procedure, but they were not observed before 2 weeks (Fig. 2D). To find the origin of the transcranial vessels, we selectively injected blue dye via the ECAs. The blue dye that was injected into the bilateral ECAs was visualized grossly only in the cerebral cortex of the ipsilateral hemisphere in which the MBD procedure was performed (Fig. 2E).

3.3. Enhanced vessel maturation with EPO pre-treatment

We evaluated the capacity for angiogenesis and arteriogenesis through administration of a combination therapy (EPO pre-treatment and an MBD procedure) into transcranial anastomoses (Fig. 3). To confirm our hypothesis of reverse vessel formation initiated in the scalp tissue, we assessed the areas within the RECA-1 positive hemispheres at 1 and 3 months, according to the distance from the cortical surface in both (Fig. 3A–E). Compared to those in the contralateral hemisphere in which the MBD procedure was not performed, the RECA-1 positive vessels in the superficial cortical layer (0 to 400 μm in depth) were significantly increased in the ipsilateral hemisphere of the MBD-only group ($p = 0.0006$) and in the combined group ($p < 0.0001$) at

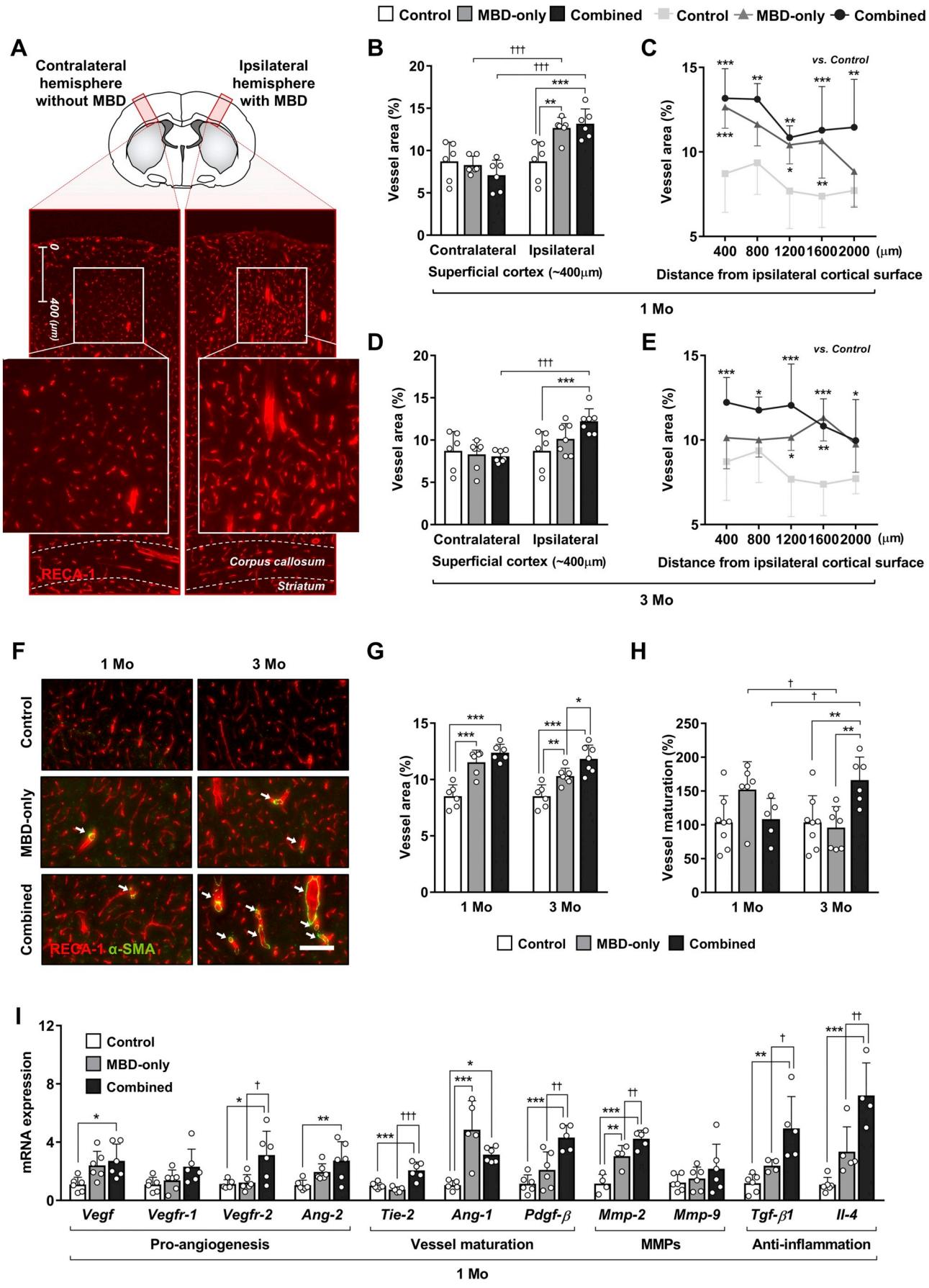

(caption on next page)

Fig. 3. Combination of EPO and MBD induces reverse angiogenesis and sustains arteriogenesis. (A) Representative image of RECA-1 positive vessels (red zone, scale bar, 400 μm) at 1 month with MBD (ipsilateral hemisphere) or without MBD (contralateral hemisphere). (B, D) Quantification of the vessel positive area in superficial cortex, raging 0 to 400 μm, in both hemispheres at 1 month (B) and 3 months (D) after MBD procedure (n = 6 to 7 animals per group). (C, E) Quantification of the vessel positive area according to distance from cortical surface in ipsilateral hemispheres (n = 6 to 7 animals per group) at 1 month (C) and 3 months (E). (F) RECA/α-SMA double positive vessels (white arrow, mature vessel) in ipsilateral hemisphere at 1 month and 3 months (scale bar, 100 μm). (G–H) Quantification of vessel positive area (G) and maturation (H) in ipsilateral hemisphere at 1 month and 3 months (n = 6 to 7 animals per group). (I) The mRNA expression of genes related to angiogenesis, vessel maturation, MMPs, and anti-inflammation in MBD region at 1 month, as assessed by real-time RT-PCR (n = 4 to 6 animals per group). MBD-only or combined vs. control* (asterisks); MBD-only vs. combined† (daggers). $^{*}p < 0.05$, $^{**}p < 0.01$, $^{***}p < 0.001$, $^{\dagger}p < 0.05$, $^{\dagger\dagger}p < 0.01$, $^{\dagger\dagger\dagger}p < 0.001$. Mo = month. (For interpretation of the references to colour in this figure legend, the reader is referred to the web version of this article.)

1 month (Fig. 3B). The number of RECA-1 positive vessels in the MBD-only and combined groups was higher than that in the control group in all cortical layers (0 to 2000 μm in depth) despite the lack of a significant difference between the MBD-only and combined groups (Fig. 3C). At 3 months, the number of RECA-1 positive vessels in the superficial cortical layer (0 to 400 μm) was significantly increased in the ipsilateral hemisphere in the combined group ($p < 0.0001$), but not in the MBD-only group ($p = 0.1847$), compared to that in the contralateral hemisphere (Fig. 3D). Compared with the control group, the combined group had a significantly higher number of RECA-1 positive vessels at depths ranging from 0 to 1200 μm (Fig. 3E).

To visualize functional aspects of transcranial vessels, we performed and observed postmortem cerebral angiography with transcardial India ink-gelatin solution injection (Supplementary Fig. 6). As compared with control group, ipsilateral MBD region (with cutting transcranial vessels for brain extraction) grossly showed little superficial vasculature in MBD-only and combined groups due to their more transcranial anastomoses. In coronal section from the extracted brain, ipsilateral MBD region had more tendency of functional vessels in MBD-only and combined group, as compared with contralateral hemisphere without MBD.

To compare the RECA-1 positive vessel area (angiogenesis) in the ipsilateral hemisphere in each of the groups at 1 and 3 months, we analyzed the regions at depths ranging from 0 to 1200 μm. (Fig. 3F–H). Compared to that in the control group, the RECA-1 positive vessel area was significantly larger in the MBD-only and combined groups at 1 month (MBD-only, $p < 0.0001$; combined, $p < 0.0001$) and 3 months (MBD-only, $p = 0.007$; combined, $p < 0.0001$). Interestingly, the combined group had a significantly larger RECA-1 positive area at 3 months (combined vs. MBD-only, $p = 0.0182$) (Fig. 3G). To evaluate vessel maturation (arteriogenesis), we concomitantly performed double-staining immunofluorescence using RECA-1 as a vessel marker and α-SMA as a mature vessel marker. The matured vessels with RECA-1 and α-SMA double-positive cells were significantly increased in the combined group at 3 months (combined vs. control, $p = 0.0097$; combined vs. MBD-only, $p = 0.0046$), although they were not different in all groups at 1 month. Over time, vessel maturation increased in the combined group ($p = 0.0403$) but gradually reduced ($p = 0.028$) in the MBD-only group (Fig. 3H).

To interpret these phenomena, we analyzed the genes related to angiogenesis, vessel maturation, MMPs, and anti-inflammation at 1 month after the MBD procedure using real-time PCR. The combined group (vs. control) showed a significantly high expression of the genes for vascular endothelial growth factor (*Vegf*) ($p = 0.0206$), *Vegf receptor-2* ($p = 0.0184$), angiopoietin (*Ang*)*-1* ($p = 0.0269$), *Ang-2* ($p = 0.0092$), *Tie-2* ($p = 0.0007$), platelet derived growth factor (*Pdgf*)-β ($p = 0.0002$), matrix metalloproteinase (*Mmp*)*-2* ($p < 0.0001$), transforming growth factor (*Tgf*)*-β1* ($p = 0.0016$), and interleukin (*Il*)*-4* ($p = 0.0001$) in the MBD region, while the MBD-only group showed a significantly high expression of the genes *Ang*-1 ($p = 0.0005$) and *Mmp-2* ($p = 0.0056$). The combined group (vs. the MBD-only group) also showed a significant increase in the gene expression of *the Vegf receptor-2* ($p = 0.0186$), *Tie-2* ($p = 0.0001$), *Pdgf*-β ($p = 0.0043$), *Mmp-2* ($p = 0.0488$), *Tgf-β1* ($p = 0.037$), and *Il-4* ($p = 0.0071$). These findings indicate that combination therapy with the MBD procedure and EPO pre-treatment facilitates angiogenesis and arteriogenesis (Fig. 3I).

3.4. Inflammation mitigation after EPO pre-treatment

We observed a significant decrease of BBB permeability in combined group at 1 day ($p = 0.0104$) and 4 days ($p = 0.0401$), compared to MBD-only group, indicating that EPO pre-treatment could attenuated the BBB breakdown after MBD procedure (Supplementary Fig. 5).

To assess the anti-inflammatory response to EPO pre-treatment after the MBD procedure (Fig. 4), we examined the activation status and morphology of resident microglia and infiltrating macrophage using their common marker at 1 day, 4 days, and 2 weeks after the MBD procedure. The MBD-only group showed significantly prominent microglia/macrophage activation at 1 day ($p = 0.0118$), whereas the combined group showed prominent microglia/macrophage activation at 4 days ($p = 0.0362$), suggesting that EPO pre-treatment with the MBD procedure could suppress early microglia/macrophage activation (MBD-only group vs. combined group, $p = 0.0121$ at 1 day) (Fig. 4A-B).

Consistent with these findings, we analyzed the genes associated with microglia/macrophage activation at 1 day, 4 days, and 2 weeks after the MBD procedure using real-time PCR, specifically the pro-inflammatory, anti-inflammatory, and MMPs genes (Fig. 4C–E). At 1 day after the MBD procedure, compared to the control group, the MBD-only group showed a significant increase in the pro-inflammatory factors (*Tnf-α*, $p = 0.0007$; *Il-6*, $p = 0.0036$; *Il-1β*, $p = 0.0005$), whereas compared to the MBD-only group, the combined group had an attenuation of those factors (*Tnf-α*, $p = 0.0008$; *Il-6*, $p = 0.025$; *Il-1β*, $p = 0.0012$) (Fig. 4C). At 4 days after the MBD procedure, the combined group showed a significant increase in the gene expression of *Il-1β*, among the pro-inflammatory factors (combined vs. control, $p = 0.0392$), and *Tgf-β1*, among the anti-inflammatory factors (combined vs. control, $p = 0.0018$; combined vs. MBD-only, $p = 0.0026$) (Fig. 4D). At 2 weeks after the MBD procedure, the MBD-only group (compared to controls) showed a significant increase in the gene expression of *Il-6* ($p = 0.0401$) and *Il-4* ($p = 0.0151$), and the combined group (compared to controls) showed a significant increase in the gene expression of *Il-6* ($p = 0.0015$), *Il-1β* ($p = 0.0464$), *Tgf-β1* ($p = 0.0083$), *Il-4* ($p = 0.047$), and *Mmp-2* ($p = 0.0001$). The combined group also showed a significantly higher expression of genes *Tgf-β1* ($p = 0.0054$) and *Mmp-2* ($p < 0.0001$) than in the MBD-only group (Fig. 4E). These findings can be explained by the premise that EPO pre-treatment exerts anti-inflammatory and tissue remodeling properties (MBD-performed environment enrichment) by inhibiting microglia/macrophage activation and releasing related factors (i.e., TGF-β1 and MMP-2) until 2 weeks.

3.5. Angiogenesis and arteriogenesis mediation with TGF-β1 and MMP-2 after EPO treatment

We performed in vitro experiments using HUVECs and HAoSMCs to elucidate the effects of EPO on angiogenesis and arteriogenesis (Fig. 5). To determine whether EPO could promote angiogenesis in vitro, HUVECs were incubated with rhEPO (0, 1, 10, and 100 IU/mL) for 24 h, and capillary-like tube formation was observed. Compared to that at 0, 1, and 100 IU/mL, incubation of HUVECs with rhEPO at 10 IU/mL for 24 h significantly increased the capillary-like tube formation, indicating that 10 IU/ml EPO can promote angiogenesis in vitro (Fig. 5A–C). Treatment of HUVECs in the presence or absence of minocycline (MIC, TGF-β1 and MMP-2 inhibitor), SB431542 (TGF-β1 inhibitor), and ARP-

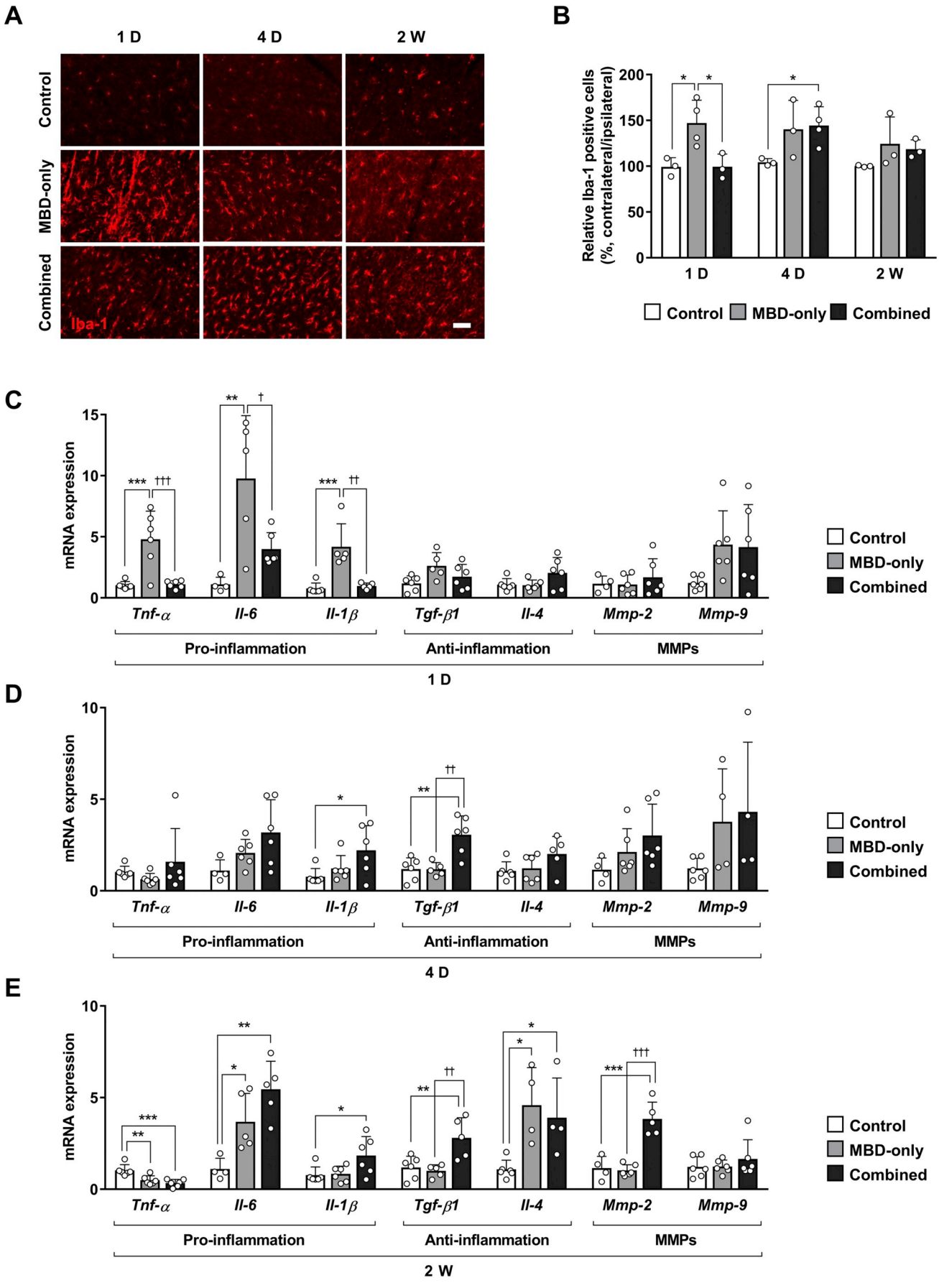

(caption on next page)

Fig. 4. EPO pretreatment mitigates inflammatory responses after MBD procedure. (A) Iba-1 positive microglia/macrophage (red) at 1 day, 4 days, and 2 weeks after MBD procedure (scale bar, 25 μm). (B) Quantification of the relative microglia/macrophage activation, as assessed by the percentage of Iba-1 positive cells in ipsilateral cortex to contralateral cortex (n = 6 to 8 animals per group). (C–E) The mRNA expression of genes related to pro-inflammation, anti-inflammation, and MMPs in MBD region at 1 day (C), 4 days (D), and 2 weeks (E), as assessed by real-time RT-PCR (n = 4 to 6 animals per group). MBD-only or combined vs. control* (asterisks); MBD-only vs. combined† (daggers). $^{*}p < 0.05$, $^{**}p < 0.01$, $^{***}p < 0.001$, $^{\dagger}p < 0.05$, $^{\dagger\dagger}p < 0.01$, $^{\dagger\dagger\dagger}p < 0.001$. D = day; W = week.

100 (MMP-2 inhibitor) resulted in significant prevention of EPO-induced tube formation (Fig. 5D). Quantitative analysis showed that both the total tube length and the number of branching points in HUVECs with EPO were significantly inhibited after treatment with MIC, SB431542, and ARP-100 (total tube length: MIC, $p < 0.0001$; SB431542, $p = 0.0008$; ARP-100, $p = 0.0238$; branching points: MIC, $p < 0.0001$; SB431542, $p = 0.0127$; ARP-100, $p = 0.0167$) (Fig. 5F-G). These data suggested that TGF-β1 and MMP-2 were essential for EPO-induced angiogenesis in vitro.

To further investigate the effects of paracrine factors secreted by EPO-treated HUVECs on SMCs migration, which is critical step in the process of arteriogenesis, we performed a wound healing assay in HAoSMCs in the conditioned medium of HUVECs (HUVECs-CM) (Fig. 5E). There was no difference in the migration of HAoSMCs in HUVECs-CM with or without EPO into the scratch area ($p = 0.9695$). In contrast, migration inhibition of HAoSMCs was observed after treatment with MIC ($p = 0.0345$), SB431542 ($p = 0.0021$), and ARP-100 ($p = 0.0142$) (Fig. 5H). These data suggested that TGF-β1 and MMP-2, which are secreted by ECs during EPO-induced angiogenesis, promote vascular maturation by facilitating migration of SMCs.

3.6. Suppression of vessel maturation through minocycline administration

We sought to examine whether suppression of inflammation and MMPs could inhibit reverse arteriogenesis (Fig. 6). To broadly inhibit acute inflammation and suppress MMPs in the subacute phase, we used minocycline (MIC), an inhibitor of microglia/macrophage activation and MMP expression, until 2 weeks. The antagonistic efficacy of MIC was verified by analyzing the gene expressions associated with inflammation and MMPs at 1 day and 2 weeks after the MBD procedure (Fig. 6A). At 1 day after the MBD procedure, the MBD-only + MIC group (vs. MBD-only) showed substantially decreased gene expressions of *Tnf-α* ($p = 0.0001$), *Il-6* ($p = 0.0007$), and *Il-1β* ($p = 0.0001$), which were at levels similar to those in the combined group with EPO pre-treatment (Fig. 6B). At 2 weeks after the MBD procedure, MIC treatment suppressed the increase in gene expressions in the MBD-only group (MBD-only vs. MBD-only + MIC, *Il-6*, $p = 0.0051$; *Il-4*, $p = 0.0478$) as well as the combined group (Combined vs. Combiend + MIC, *Il-1β*, $p = 0.0437$; *Tgf-β1*, $p = 0.0009$; *Mmp-2*, $p < 0.0001$) (Fig. 6C). These results indicated that MIC suppresses pro-inflammatory factors, which could be inhibited by EPO treatment at 1 day, and also tissue regenerating factors (TGF-β1 and MMP-2), which were increased by EPO treatment at 2 weeks. Histologically, we analyzed the RECA-1 positive vessel area (angiogenesis) and vessel maturation (arteriogenesis) at 3 months (Fig. 6E-F). MIC treatment significantly decreased the vessel area in the MBD-only + MIC group (vs. MBD-only, $p = 0.0075$) and the combined + MIC group (vs. combined, $p = 0.0099$) (Fig. 6E). It also substantially decreased vessel maturation in the combined + MIC group (vs. combined, $p = 0.0414$) not the MBD-only + MIC group (Fig. 6F). These results suggest that tissue regenerating factors (i.e., TGF-β1 and MMP-2) are presumably responsible for the key mediators of tissue remodeling in the reverse arteriogenesis through combination therapy.

4. Discussion

Current study is a reverse translational research that extrapolates our bedside results to bench through systematized basic experiments. Our experimental findings illustrate that reverse arteriogenesis through a cranial hole by the MBD procedure was successfully induced from the healthy extracranial vascular system and then augmented even further with EPO pre-treatment in a bICAL rat model. Transcranial vascular anastomosis was grossly observed 2-weeks following the MBD procedure. In the detailed histological analyses, angiogenesis and arteriogenesis were significantly prominent in the superficial cortex. The MBD hemisphere showed a significant increase in inflammatory and proangiogenic markers. However, systemic EPO administration mitigated regional inflammation and boosted focal arteriogenesis. On the basis of the in vitro *and* in vivo experiments, the increase in arteriogenesis was suppressed after MIC administration by inhibiting the expression of TGF-β1 and MMP-2.

4.1. MBD-induced reverse arteriogenesis

Our experiments showed that the MBD procedure induced reverse arteriogenesis without additional neuronal death. Revascularization surgery from the extracranial vascular system has been clinically proven to treat progressive cerebrovascular occlusive disorders like Moyamoya disease with insufficient intracranial blood flow (Pandey and Steinberg, 2011). However, there is a potential risk of relatively high rates of postoperative stroke and complications after revascularization surgery. Nonetheless, this method cannot guarantee stable new vessel formation through the trans-dural collaterals from the enriched extracranial environment.

4.2. Extracranial and intracranial angiogenic modulation by MBD procedure

In this study, successful transcranial vascular anastomosis emerged in MBD-only and combined groups at around 2 weeks after ligation surgery (subacute period). Theoretically, a poor intracranial milieu in cerebrovascular occlusive disease would be less favorable for new vascular network formation than the enriched extracranial milieu (Hecht et al., 2015). The MBD procedure provides a simple detour from the cranial protective layers between the extracranial and intracranial carotid circulation systems with different environments (Hong et al., 2018). We believe that the newly-formed transcranial vascular anastomosis can be closely associated with a normal wound healing process such as inflammation, proliferation, and angiopoietic remodeling after external injury (Guo and Dipietro, 2010; Russo et al., 2018). In detail, we observed such vascular networks when the galea and periosteum were reconstructed toward the defected skull at 2 weeks, which can be explained by the restorative properties of the periosteum during healing of the bony defect (Ferretti and Mattioli-Belmonte, 2014). Periosteum is a layer of a vascular connective tissue covering the surfaces of bones, and its clinical application has been reported as a pivotal tissue with wound-repair function in the specified situations such as bone fracture (Wang et al., 2019), bone defection (Ferretti and Mattioli-Belmonte, 2014), and scalp avulsion (Furlanetti et al., 2010). Further experiments for the extracranial wound-healing processes are warranted to clarify the impact of the MBD procedure in the extracranial milieu. Furthermore, we observed transient BBB disruption for 2 weeks after the ipsilateral MBD procedure without parenchymal damage to the brain. Although VEGF is an agent with vascular permeability and is a potent angiogenic facilitator, its long-term exposure can be deleterious, leading to a chronic impairment of the BBB, vessel regression, and increased inflammation (Nag, 2002). Therefore, new vessel formation by temporary mechanical disruption of the cranial protective layers via the MBD procedure seems to be associated with transient angiogenic

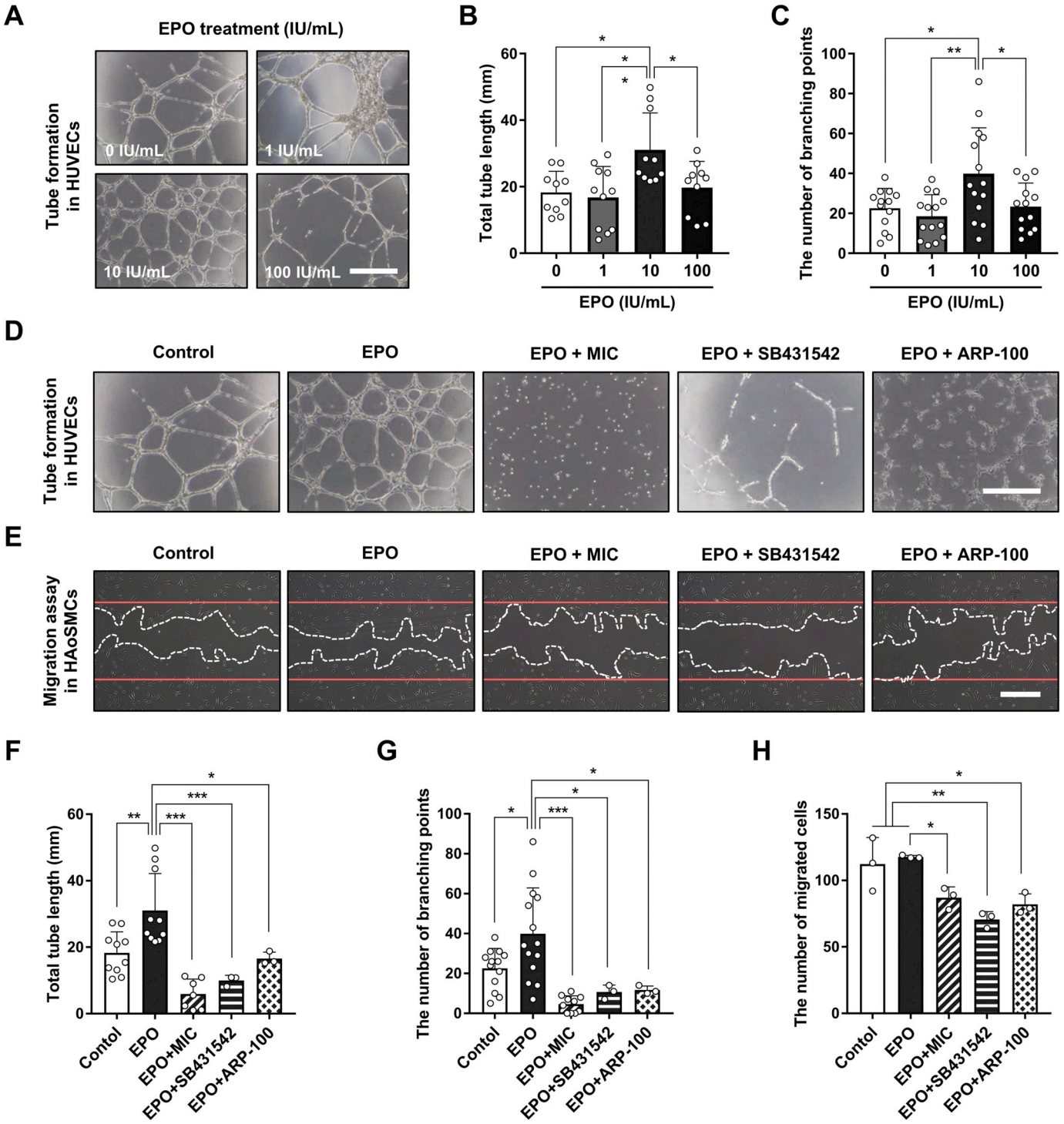

Fig. 5. In vitro experiments show that angiogenesis and arteriogenesis after EPO treatment are prohibited by TGF-β1 and MMP-2 inhibitors. (A) Tube formation in HUVECs culture after 24 h of incubation with 1, 10, and 100 IU/mL EPO (scale bar, 500 μm). (B–C) Quantification of total tube length (B) and the number of branching points (C) in tube formation of HUVECs culture (n = 10 to 14 from four independent experiments). (D) Tube formation in HUVECs culture at 24 h after incubation with 10 IU/mL EPO in the presence or absence of 10 μM MIC (TGF-β1 and MMP-2 inhibitor), 10 μM SB431542 (TGF- β1 inhibitor), and 5 μM ARP-100 (MMP-2 inhibitor). (E) Wound migration assay in HAoSMCs culture at 8 h after incubation with conditioned media collected from EPO-treated HUVECs with or without inhibitors. (F-G) Quantification of total tube length (F) and the number of branching points (G) in tube formation of HUVECs culture (n = 3 to 14 from four independent experiments). (H) Quantification of HAoSMCs migration, as assessed by counting of migrated cells into wounded area at 8 h (n = 3 from three independent experiments). Scale bar, 500 μm. $^{*}p < 0.05$, $^{**}p < 0.01$, $^{***}p < 0.001$.

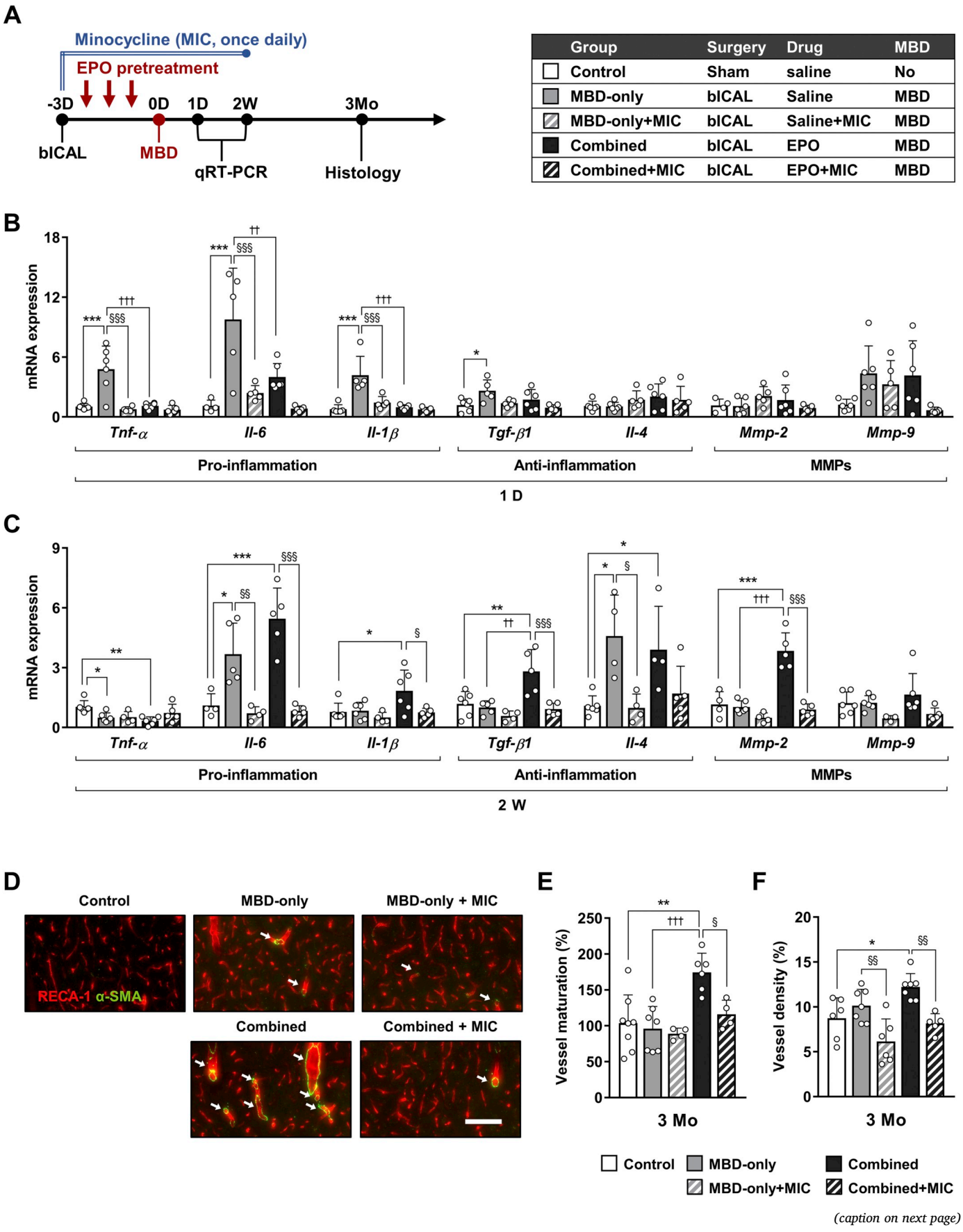

(caption on next page)

Fig. 6. Minocycline (MIC) inhibits the reverse arteriogenesis augmented by combined therapy. (A) Schematic diagram of the experimental process for MIC co-administration. (B–C) The mRNA expression of genes related to pro-inflammation, anti-inflammation, and MMPs in MBD region at 1 day (B) and 2 weeks (C), as assessed by real-time RT-PCR (n = 4 to 5 animals per group, MBD-only or combined vs. control* (asterisks); MBD-only vs. combined† (daggers); without MIC vs. with MIC§ (section marks)). (D) RECA/α-SMA double positive vessels (white arrow, mature vessel) in ipsilateral hemisphere at 3 months (scale bar, 100 μm). (E-F) Quantification of vessel positive area (E) and maturation (F) in ipsilateral MBD hemisphere at 3 months (n = 4 to 8 animals per group). $^{*}p < 0.05$, $^{**}p < 0.01$, $^{***}p < 0.001$, $^{\dagger}p < 0.05$, $^{\dagger\dagger}p < 0.01$, $^{\dagger\dagger\dagger}p < 0.001$, $^{\S}p < 0.05$, $^{\S\S}p < 0.01$, $^{\S\S\S}p < 0.001$. D = day; W = week; Mo = month.

Sequential change in intracranial milieus	*Step 1:* Regional hypoxia	*Step 2:* Combination Tx	*Step 3:* Angiogenesis	*Step 4:* Arteriogenesis
Illustration	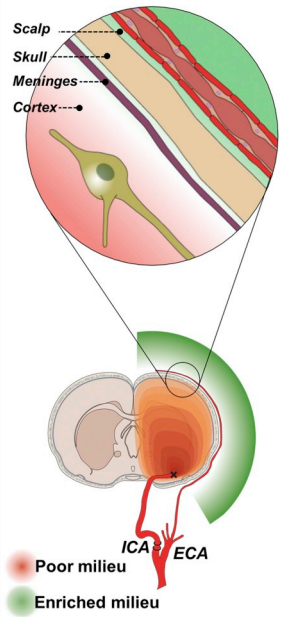	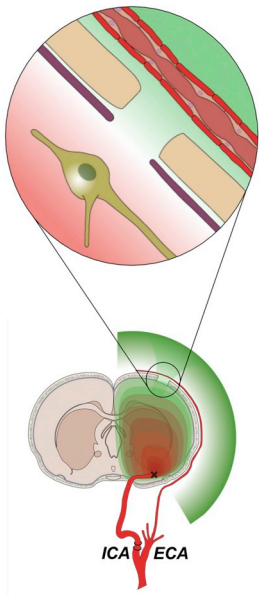	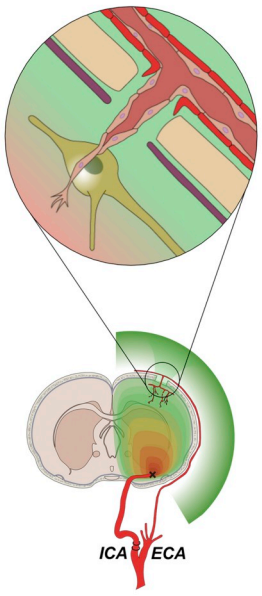	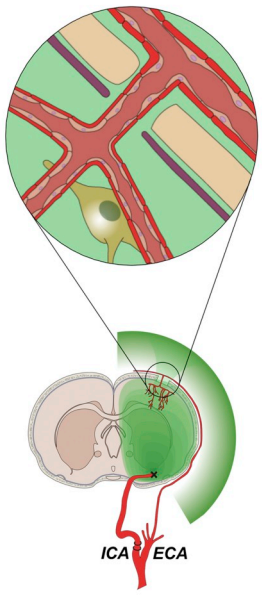
Phase	• Baseline	• Acute (< 2W)	• Subacute (2W to 1Mo)	• Chronic (after 1 Mo)
Procedure	• Regional ischemic condition by bilateral ICA ligation	• Angiopoietic booster (ie. EPO) • MBD procedure	-	-
Potential mediators	• Poor milieu with intracranial perfusion impairment • Enriched extracranial milieu	• Transient BBB breakdown • Inflammation attenuation • Increase of hematocrit	• Angiogenic factors (ie. VEGF, VEGFR-2, Ang-2) • Remodeling factor (ie. MMP-2, TGF-β1)	• Maturation factors (ie. Tie-2 and PDGF-β)
Possible mechanism	-	• EPO as arteriogenic booster • Vascular detour by minimally-invasive MBD from extracranial system	• Periosteal healing • BBB stabilization • Aberrant trasdural anastomosis	• Maturation of newly formed vessels

Fig. 7. Summary of our experiments depicting the reverse arteriogenesis boosted by combined therapy.

modulation from the enriched extracranial milieu. This MBD concept might be translated to various ischemic diseases, such as ischemic stroke, coronary artery disease, and peripheral artery occlusive disease in the future.

4.3. Intracranial milieu modulation by EPO pre-treatment

Our experiment demonstrated that combination therapy (MBD-EPO treatment) would be more beneficial than MBD-only because it led to a decrease in inflammation and an increase in vessel formation and maturation. In numerous experiments, EPO has been neuroprotective with anti-inflammatory properties (Bond and Rex, 2014). As such, our results would be in line with the previous observations. It would be interesting to determine whether combination therapy could induce a significant enhancement of vessel maturation. Additionally, knowledge of whether its augmentation was impeded by prolonged MIC administration, representing a down-regulation of TGF-β1 and MMP-2, would also be valuable. We believe that combination therapy can be synergistic in two beneficial ways, inflammation attenuation and matured vessel enhancement.

4.3.1. Inflammation attenuation

MBD procedure induced BBB breakdown for at least 7 days. This point suggest that peripheral macrophages infiltrate into intracranial tissues surrounding the MBD region. EPO can attenuate microglia/macrophage activation and mitigate pro-inflammatory cytokines by inhibiting neuronal death after brain injury (Bond and Rex, 2014). This was reaffirmed in our study, even in the setting of the MBD procedure. In the combined group, our data showed that EPO pre-treatment suppressed pro-inflammatory cytokines with microglia/macrophage inhibition in the acute period and increased anti-inflammatory cytokines in the later period. This appears to be in line with recent studies which

have shown that EPO promotes microglia/macrophage polarization toward anti-inflammatory M2 phenotypes in certain diseases (Wang et al., 2017). Therefore, these findings point out that EPO might act as a valuable modulator by mitigating inflammatory responses after the MBD procedure in our cerebral ischemic model.

4.3.2. Vessel maturation

We observed a conventional hematopoietic stimulation by EPO pre-treatment in the combined group, evidenced by an increase in hematocrit for 2 weeks and prolonged vessel maturity starting at 2 weeks (Supplementary table 2). Several previous studies reported that EPO administration enhanced coronary collateral development through increases in shear stress based on elevations of blood viscosity through hematopoietic boosting (Imazuru et al., 2009). In our study, the maturation of collateral vessels seemed to be associated with hematopoietic stimulation by EPO administration. We observed a sustained up-regulation of *Tgf*-β1 and *Mmp*-2 in the EPO pre-treatment group, which has been closely associated with vessel remodeling and maturation in various models (Hua et al., 2016; Roberts and Sporn, 1989; Rundhaug, 2005). In addition, our In vitro experiments demonstrated that EPO treatment enhanced capillary-like endothelial tube formation (angiogenesis) and smooth muscle cell migration (arteriogenesis), which was significantly suppressed with minocycline (MIC) (Garrido-Mesa et al., 2013). Moreover, this point also reaffirmed the in vivo experiment: MIC treatment attenuated vessel maturation with a down-regulation of *Tgf-β1* and *Mmp-2*, which is consistent with the findings from previous studies on modulating inflammation through suppression of TGF-β1 and MMP-2 by MIC (Ataie-Kachoie et al., 2013; Garrido-Mesa et al., 2013). As a consequence, we deduced that combination therapy could help reinforce angiogenic modulation by enriching shear stress, TGF-β1, and MMP-2 in intracranial environments.

4.4. Intracranial and extracranial milieu modulation by combination therapy

Our study provides further physiologic insight into the facilitation of reverse arteriogenesis by combination therapy in a bilateral ischemic rat model with cerebral perfusion impairment (Fig. 7). To summarize, we described several stepwise processes. *Step 1 (A, baseline):* Intracranial hypoxia is attributed to bICAL, which promotes the relatively good extracranial milieu to initiate regional revascularization, because this model has a mechanical barrier between the intracranial and extracranial cavities. *Step 2 (B, acute):* A simple burr hole procedure breaks the barrier between the two distinctive milieus (Hong et al., 2018). An extracranial wound healing process initiates vessel sprouting from the quiescent brigade of the extracranial endothelium, while circulating angiogenic cytokines form a chemotactic gradient. *Step 3 (C, subacute)*: Although perfusion impairments inside the brain can be restored through successful trans-dural collaterals (Hong et al., 2016), such newly-formed vessels tended to vanish more easily in the MBD-only group than in the combined group, which has also been seen in an indirect bypass model without additional drugs. *Step 4 (D, chronic):* EPO pre-treatment appears to promote arteriogenesis by enhancing matured cell arteriogenesis, rather than via aberrant angiogenesis. This might be attributed to elevated expressions of genes related to anti-inflammatory cytokines, angiogenesis, and vessel maturation. Moreover, elevated expressions of *Tgf-β1* and *Mmp-2* might play key roles in promoting maturation processes such as the “stabilization” of cell junctions and tight pericyte recruitment (arteriogenesis) (Hua et al., 2016). As a consequence, our data demonstrate that combination therapy would be more beneficial, as EPO treatment mitigates the elevation in the inflammatory process after the MBD procedure.

5. Conclusions

In conclusion, our data suggest that the combination method is feasible for generalizing this new concept of reverse arteriogenesis without aberrant angiogenic regression during the early phase of wound healing. This might be because of the possibility of upregulation of tissue regenerating determinants or downregulation of hazard inflammation determinants in the acute and subacute phases of the stroke model.

Declaration of Competing Interests

All authors have no conflict of interest to declare.

Acknowledgements

This research was supported by a grant of the Korea Health Technology R&D Project through the Korea Health Industry Development Institute (KHIDI), funded by the Ministry of Health & Welfare, Republic of Korea (grant number: HI16C2227).

Appendix A. Supplementary data

Supplementary data to this article can be found online at https://doi.org/10.1016/j.nbd.2019.104538.

References

Adams Jr., H.P., Nudo, R.J., 2013. Management of patients with stroke: is it time to expand treatment options? Ann. Neurol. 74, 4–10. https://doi.org/10.1002/ana.23948.

Ataie-Kachoie, P., et al., 2013. Minocycline targets the NF-kappaB Nexus through suppression of TGF-beta1-TAK1-IkappaB signaling in ovarian cancer. Mol. Cancer Res. 11, 1279–1291. https://doi.org/10.1158/1541-7786.Mcr-13-0239.

Bernaudin, M., et al., 2000. Neurons and astrocytes express EPO mRNA: oxygen-sensing mechanisms that involve the redox-state of the brain. Glia 30, 271–278.

Bond, W.S., Rex, T.S., 2014. Evidence that erythropoietin modulates neuroinflammation through differential action on neurons, astrocytes, and microglia. Front. Immunol. 5, 523. https://doi.org/10.3389/fimmu.2014.00523.

Brines, M., Cerami, A., 2005. Emerging biological roles for erythropoietin in the nervous system. Nat. Rev. Neurosci. 6, 484–494. https://doi.org/10.1038/nrn1687.

Cho, W.S., et al., 2014. Long-term outcomes after combined revascularization surgery in adult moyamoya disease. Stroke 45, 3025–3031. https://doi.org/10.1161/strokeaha.114.005624.

Cuccione, E., et al., 2016. Cerebral collateral circulation in experimental ischemic stroke. Exp. Transl. Stroke Med. 8, 2. https://doi.org/10.1186/s13231-016-0015-0.

Dirnagl, U., et al., 1999. Pathobiology of ischaemic stroke: an integrated view. Trends Neurosci. 22, 391–397.

Ferretti, C., Mattioli-Belmonte, M., 2014. Periosteum derived stem cells for regenerative medicine proposals: boosting current knowledge. World J. Stem Cells 6, 266–277. https://doi.org/10.4252/wjsc.v6.i3.266.

Furlanetti, L.L., et al., 2010. Multiple cranial burr holes as an alternative treatment for total scalp avulsion. Childs Nerv. Syst. 26, 745–749. https://doi.org/10.1007/s00381-010-1145-7.

Garrido-Mesa, N., et al., 2013. Minocycline: far beyond an antibiotic. Br. J. Pharmacol. 169, 337–352. https://doi.org/10.1111/bph.12139.

Guo, S., Dipietro, L.A., 2010. Factors affecting wound healing. J. Dent. Res. 89, 219–229. https://doi.org/10.1177/0022034509359125.

Hamauchi, S., et al., 2015. Review of past and present research on experimental models of moyamoya disease. Brain Circl. 1, 88–96. https://doi.org/10.4103/2394-8108.166377.

Hecht, N., et al., 2015. Myoblast-mediated gene therapy improves functional collateralization in chronic cerebral hypoperfusion. Stroke 46, 203–211. https://doi.org/10.1161/strokeaha.114.006712.

Hong, J.M., et al., 2016. Hemodynamic contribution of transdural collateral flow in adult patients with Moyamoya disease. Neurol. Sci. 37 (12), 1969–1977. https://doi.org/10.1007/s10072-016-2700-0.

Hong, J.M., et al., 2018. Feasibility of multiple Burr hole with erythropoietin in acute Moyamoya patients. Stroke 49, 1290–1295. https://doi.org/10.1161/strokeaha.117.020566.

Hua, Y., et al., 2016. MMP-2 is mainly expressed in arterioles and contributes to cerebral vascular remodeling associated with TGF-beta1 Signaling. J. Mol. Neurosci. 59,

317–325. https://doi.org/10.1007/s12031-015-0687-2.
Imazuru, T., et al., 2009. Erythropoietin enhances arterioles more significantly than it does capillaries in an infarcted rat heart model. Int. Heart J. 50, 801–810.
Jana, S., et al., 2016. Regulation of matrix Metalloproteinase-2 activity by COX-2-PGE2-pAKT Axis promotes angiogenesis in endometriosis. PLoS ONE 11, e0163540. https://doi.org/10.1371/journal.pone.0163540.
Janmaat, M.L., et al., 2010. Erythropoietin accelerates smooth muscle cell-rich vascular lesion formation in mice through endothelial cell activation involving enhanced PDGF-BB release. Blood 115, 1453–1460. https://doi.org/10.1182/blood-2009-07-230870.
Jaquet, K., et al., 2002. Erythropoietin and VEGF exhibit equal angiogenic potential. Microvasc. Res. 64, 326–333.
Jerndal, M., et al., 2010. A systematic review and meta-analysis of erythropoietin in experimental stroke. J. Cereb. Blood Flow Metab. 30, 961–968. https://doi.org/10.1038/jcbfm.2009.267.
Jung, H.J., et al., 2014. Minocycline inhibits angiogenesis in vitro through the translational suppression of HIF-1alpha. Arch. Biochem. Biophys. 545, 74–82. https://doi.org/10.1016/j.abb.2013.12.023.
Liu, J., et al., 2014. Vascular remodeling after ischemic stroke: mechanisms and therapeutic potentials. Prog. Neurobiol. 115, 138–156. https://doi.org/10.1016/j.pneurobio.2013.11.004.
Ma, J., et al., 2007. MCP-1 mediates TGF-beta-induced angiogenesis by stimulating vascular smooth muscle cell migration. Blood 109, 987–994. https://doi.org/10.1182/blood-2006-07-036400.
Nag, S., 2002. The blood-brain barrier and cerebral angiogenesis: lessons from the cold-injury model. Trends Mol. Med. 8, 38–44.
Nemoto, E.M., et al., 2003. Stages and thresholds of hemodynamic failure. Stroke 34, 2–3.
Ohta, H., et al., 1997. Chronic cerebral hypoperfusion by permanent internal carotid ligation produces learning impairment without brain damage in rats. Neuroscience 79, 1039–1050.
Pandey, P., Steinberg, G.K., 2011. Neurosurgical advances in the treatment of moyamoya disease. Stroke 42, 3304–3310. https://doi.org/10.1161/strokeaha.110.598565.
Roberts, A.B., Sporn, M.B., 1989. Regulation of endothelial cell growth, architecture, and matrix synthesis by TGF-beta. Am. Rev. Respir. Dis. 140, 1126–1128. https://doi.org/10.1164/ajrccm/140.4.1126.
Rundhaug, J.E., 2005. Matrix metalloproteinases and angiogenesis. J. Cell. Mol. Med. 9, 267–285.
Russo, M.V., et al., 2018. Distinct myeloid cell subsets promote meningeal remodeling and vascular repair after mild traumatic brain injury. Nat. Immunol. 19, 442–452. https://doi.org/10.1038/s41590-018-0086-2.
Scott, R.M., Smith, E.R., 2009. Moyamoya disease and moyamoya syndrome. N. Engl. J. Med. 360, 1226–1237. https://doi.org/10.1056/NEJMra0804622.
Subiros, N., et al., 2012. Erythropoietin: still on the neuroprotection road. Ther. Adv. Neurol. Disord. 5, 161–173. https://doi.org/10.1177/1756285611434926.
Wang, L., et al., 2004. Treatment of stroke with erythropoietin enhances neurogenesis and angiogenesis and improves neurological function in rats. Stroke 35, 1732–1737. https://doi.org/10.1161/01.STR.0000132196.49028.a4.
Wang, S., et al., 2017. Erythropoietin protects against rhabdomyolysis-induced acute kidney injury by modulating macrophage polarization. Cell Death Dis. 8, e2725. https://doi.org/10.1038/cddis.2017.104.
Wang, X., et al., 2019. PDGF modulates BMP2-induced Osteogenesis in periosteal progenitor cells. JBMR Plus. 3, e10127. https://doi.org/10.1002/jbm4.10127.
Zhang, Z.G., Chopp, M., 2009. Neurorestorative therapies for stroke: underlying mechanisms and translation to the clinic. Lancet Neurol. 8, 491–500. https://doi.org/10.1016/s1474-4422(09)70061-4.